Available online at www.sciencedirect.com
ScienceDirect
Marine and Petroleum Geology 26 (2009) 249–258
Marine and Petroleum Geology
www.elsevier.com/locate/marpetgeo

Salt rollers: Structure and kinematics from analogue modelling

Jean-Pierre Brun*, Thomas P.-O. Mauduit[1]

Géosciences Rennes UMR 6118 CNRS, University Rennes 1, 35042 Rennes Cedex, France

Received 1 May 2007; received in revised form 21 January 2008; accepted 3 February 2008

Abstract

Salt rollers are low-amplitude deflections of the upper surface of a salt layer which occur below zones of normal faulting in the overlying sediments. They are widely recognised in association with tilted blocks or listric fault rollover systems. Laboratory experiments on brittle ductile models made of sand and silicone putty are used to study the modes of development, the external shape and the internal structures of these salt rollers. Firstly, flow and strain patterns within décollement zones are described. Finite strain combines layer-perpendicular shortening and layer-parallel shear. Additional flow cells within rollers perturb the laminar flow of the décollement, inducing a passive folding of planar markers. The same type of flow and strain patterns occur in all types of rollers, ranging from those occurring below tilted blocks to those associated with growth faults. Finally, an analysis of roller shapes through the measurement of aspect ratios and asymmetry ratios shows that the shapes of tilted blocks rollers and growth fault rollers—which differ at initiation tend to converge with increasing deformation.

Keywords: Salt tectonics; Salt roller; Tilted blocks; Listric fault; Growth fault; Rollover

1. Introduction

The term "salt roller" has been used after Bally et al. (1981) to describe low-amplitude deflections of the upper surface of a salt layer at the lower termination of normal faults in the overlying sediments (Fig. 1). Intensive seismic exploration in sedimentary basins has demonstrated their widespread occurrence in two forms: (i) below tilted blocks (Fig. 1a) and (ii) on synthetic or antithetic growth fault/rollover systems (Fig. 1b). Typical salt rollers have two limbs, which can be either planar or upward concave, and which correspond, on one side, to the base of a fault block and, on the opposite side, to the contact of salt with either a rollover or a tilted block. Seismic images are rarely precise about the external shape of rollers (Fig. 1) and we have seen none of which show their internal structures. Although, salt rollers are extremely common, they nevertheless remain, very poorly understood: in terms of external shape, internal structure, strain pattern, kinematics and dynamics.

Laboratory experiments were performed to study the development of growth fault/rollovers systems (Mauduit and Brun, 1998; Brun and Mauduit, 2008). In all these experiments, a systematic deformation pattern developed within the models analogue of salt rollers. We present here some typical examples of modelled rollers selected among these experiments. Their external shape and their internal structures are studied in terms of progressive deformation. Experimental data are used to define the structural and kinematic significance of rollovers in salt tectonics.

2. Small-scale modelling

The models presented here consist of two-layer slabs made of Newtonian silicone putties at the base to represent salt and sand on top to represent the overlying sediments. Deformation is due to gravity alone. The silicone putties are able to flow under their own weight, but here spread beneath a sand pack that collapses by normal faults as it glides. Frontal spreading occurs when models are not inclined, and the whole model faults, spreads and glides

*Corresponding author.
E-mail addresses: jean-pierre.brun@univ-rennes1.fr (J.-P. Brun), thomas@mauduit.org (T.P.-O. Mauduit).
[1]Now at Tectonic Experts Ltd., 95 Wilton Road, Suite 3, London, SW1V 1BZ, United Kingdom.

0264-8172/$ - see front matter © 2008 Published by Elsevier Ltd.
doi:10.1016/j.marpetgeo.2008.02.002

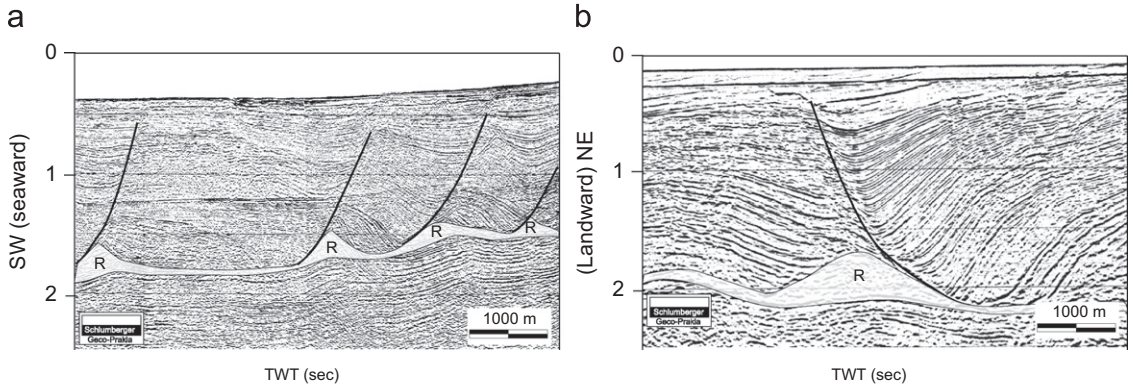

Fig. 1. Seismic images of salt rollers (R): (a) below tilted blocks and (b) below an antithetic growth fault. Seismic sections used with permission of Geco-Prakla (UK) Limited.

when the base of models is inclined a few degrees (Brun and Merle, 1985; Merle, 1986, 1989; Mauduit, 1998; Mauduit et al., 1997a, b; Mauduit and Brun, 1998; Brun and Mauduit, 2008). This kind of model has already been found useful in simulating the processes of gravity induced deformation of a sedimentary pile gliding above salt with or without synchronous sedimentation (Vendeville and Cobbold, 1987; Vendeville et al., 1987; Cobbold et al., 1989; Cobbold and Szatmari, 1991; Vendeville and Jackson 1992a, b; Gaullier et al., 1993; Ge et al., 1997; Mauduit et al., 1997a, b; McClay et al., 1998; Mauduit, 1998; Mauduit and Brun, 1998; Brun and Fort, 2004; Fort et al., 2004a, b; Brun and Mauduit, 2008). Detailed descriptions of the equipment, rheology of materials and analysis of models have already been presented in a number of previous studies (Faugère and Brun, 1984; Vendeville and Cobbold, 1987; Gaullier et al., 1993; Mauduit, 1998), which discuss scaling with regard to nature.

In the present study, some significant results concerning the structure and kinematics of salt rollers are selected from a series of more than 70 experiments.

Two specific techniques are used to study the patterns of flow and strain within the basal ductile layer. In most models, the silicone layer is made up of bars of two alternating colours but with similar viscosities arranged perpendicularly to the bulk flow direction. Vertical contacts between neighbouring bars provide efficient passive markers to reveal variations in layer-parallel shear. The analysis of passive marker deformation can only be made at the end of experiments by dissecting models in serial vertical sections parallel to the direction of gliding. In a few models, the silicone putty is transparent (PDMS, see Weijermars, 1986) with a vertical grid of passive markers arranged in the middle of the layer lying parallel to the bulk flow direction. The progressive deformation can then be monitored and photographed from the sides of the models during deformation.

3. Deformation within the decollement layer

The type of small-scale experiment described here has been shown to enable realistic simulation of many synsedimentary structures which commonly occur in deltas or within gliding sedimentary covers on passive margins (Vendeville, 1987; Vendeville and Cobbold, 1987; Cobbold et al., 1989; Vendeville and Jackson, 1992a, b; Gaullier et al., 1993; Nalpas and Brun, 1993; Ge et al., 1997; Mauduit et al., 1997a, b; McClay et al., 1998; Mauduit, 1998; Mauduit and Brun, 1998; Brun and Fort, 2004; Fort et al., 2004a, b; Brun and Mauduit, 2008): diapirs, synthetic or antithetic normal growth faults and associated rollovers, tilted blocks, horst and graben structures, turtle back structures, etc. In these experiments, faulting separates blocks in the upper brittle layer, when the brittle–ductile slab begins to collapse and glide. Since rates of displacement increase downslope, blocks tend to separate more rapidly downslope than upslope. As gliding increases, the underlying ductile layer accommodates variations in the displacement of overlying blocks. This gives rise to bulk flow patterns which combine two components (see Appendix). Layer-perpendicular shortening is due to lengthening of the upper brittle layer while the total volume of ductile material does not change. Therefore, the ductile layer thickness decreases with increasing slab length. A component of layer-parallel shear results from the downslope displacement of upper-layer blocks with respect to the underlying basement represented by the rigid base beneath the model. The resulting deformation within the ductile décollement layer is a combination of simple shear and pure shear (see Appendix).

Fig. 2a shows the distortion of initially vertical markers below a rafted block with a high aspect ratio. The amount of layer-parallel shear is obtained directly from the geometry of the deformed markers. Layer thinning is slightly greater downslope (left) than upslope (right). This observation indicates that deformation below the block combines a homogeneous component of layer-parallel shear and a component of layer-perpendicular shortening which increases downslope.

Fig. 2b shows a series of tilted blocks at the front of a slab undergoing frontal spreading to the left out of the picture. Below these tilted blocks, markers are sheared top to the front with a frontward increase in the amount of

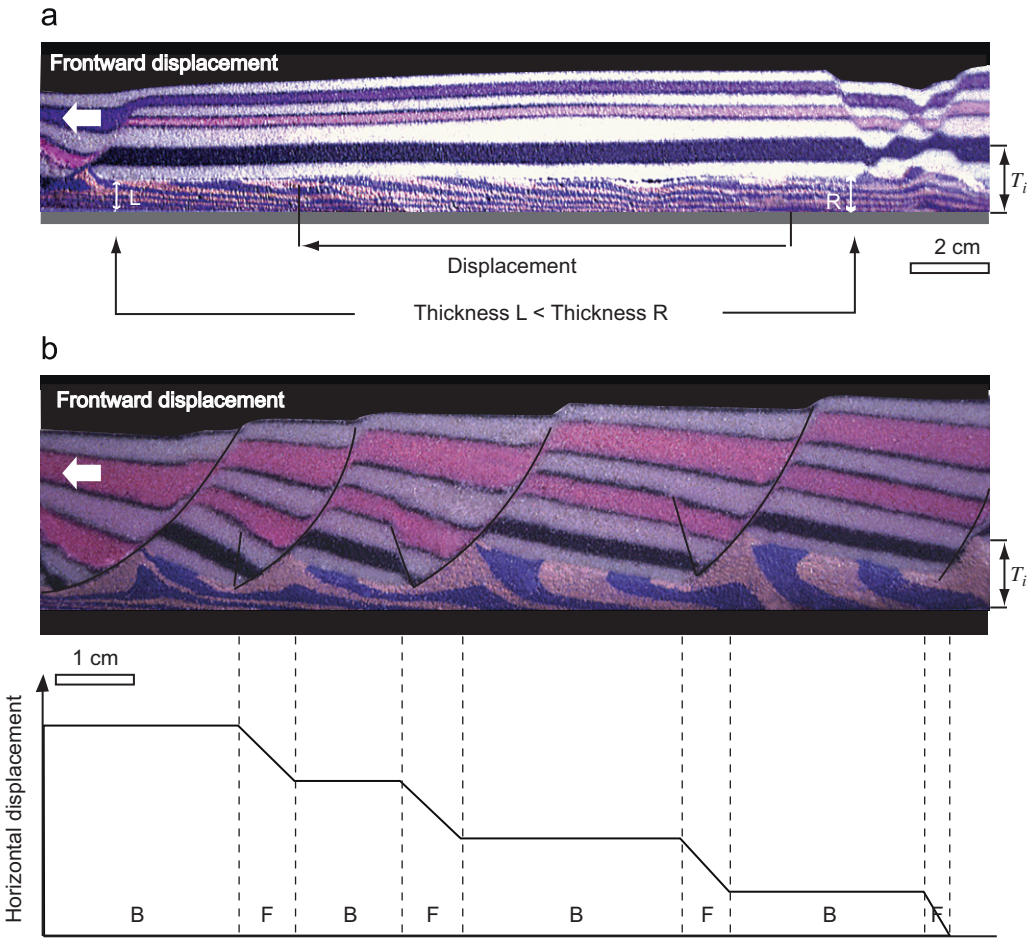

Fig. 2. Deformation within the décollement layer: (a) below a raft and (b) below a frontal series of tilted blocks. Slab front is to the left. T_i is for the initial thickness of the viscous layer.

layer-parallel displacement (see diagram in Fig. 2b) and a left frontward decrease of the mean layer thickness. In addition, markers are heterogeneously distorted below the faults of the overlying layer. The upright folding of shear markers indicates a local component of uprising flow in the triangular domains (so-called "rollers") which are bounded by a normal fault on one side and by the base of a tilted block on the opposite side. Here as well, the bulk flow pattern combines a layer-parallel shear and a layer-perpendicular shortening. The deformation of initially vertical passive markers in the ductile layer shows that the amount of layer-parallel shear increases in the sense of frontward displacement whereas the bulk layer thickness decreases. Local perturbations of this mean flow pattern occur at the intersection of the sedimentary cover faults with the ductile layer.

Fig. 3 shows an experiment carried out with transparent silicone putty (PDMS) that allows progressive strain to be observed throughout the deformation. The cross-section of Fig. 3a shows the deformation of a vertical grid of passive markers embedded in the middle of the silicone layer-parallel to the flow direction. On top of the photograph, the interface between sand and silicone is seen obliquely from below. Its wavy aspect is due to second order normal faults which affect the sand layer between two major normal faults (1 and 2 in Fig. 3a). Due to the irregular shape of the sand/silicone interface, the upper line of the grid of strain markers is partly hidden. A major fault (1) separates two domains, faulted (on the left) and unfaulted (on the right), another major fault (2) is the first of a series of faults that define tilted blocks at the unseen front of the slab to the left.

Below the unfaulted domain, initially vertical marker lines are bent horizontally with a reversal of shear sense from top to base. It could be tempting to interpret such a deformation pattern as the result of a Poiseuille flow (see Appendix) but in fact, it results from ductile layer extrusion due to layer-perpendicular shortening. Below the faulted domain, the ductile layer is strongly sheared top to the left.

The upward bending of initially horizontal markers lines indicates a component of uprising flow below major faults (1 and 2 in Fig. 3a). In Fig. 3b, which represents a later stage of development, the offset of normal fault 2 has significantly increased and a return flow has started to develop in the roller. During the early stages (Fig. 4a), the flow planes are only slightly distorted by the fault cross-cutting the brittle–ductile interface. The transition to the advanced stage (Fig. 4b), where an isolated flow cell is

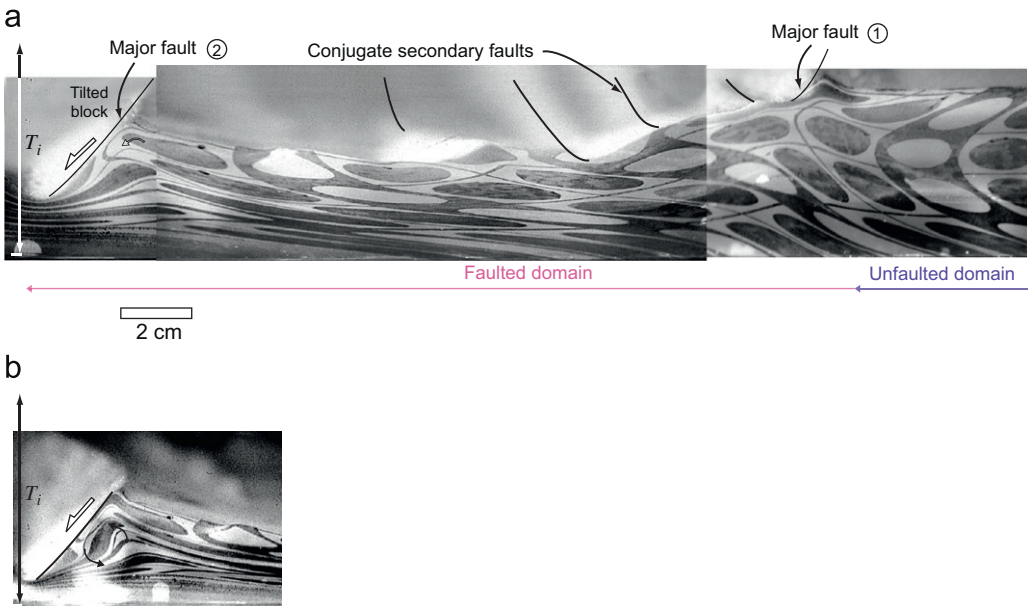

Fig. 3. Strain pattern within the décollement layer: (a) general view and (b) detailed view of the roller associated with fault 2 at a more advanced stage.

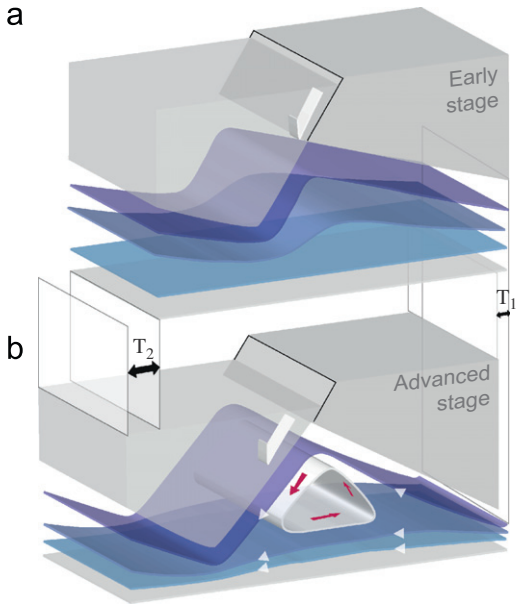

Fig. 4. Sketch diagram showing the evolution of flow lines at an early (a) and more advanced (b) stage.

present, can be attributed to the strong layer thinning occurring below the lower corner of the hangingwall block. The ductile material dragged downward by the fault cannot flow into the channel narrowing below the hangingwall block and returns within the roller.

4. Internal structures of rollers

Fig. 5a shows a model with no sedimentation during deformation. Upper layer thinning within a graben allows the lower ductile layer to uprise and to reach the surface (i.e., as a piercing diapir). Initially, vertical markers in the ductile layer are strongly sheared and rotated to a low angle of dip prior to graben opening. At the roller base and below the bounding upper layer blocks, the markers are rotated into near parallelism with the underlying basement. The internal structure of the roller, as displayed by deformed passive markers, is asymmetric, whereas its external shape is only slightly asymmetric. The ductile material—i.e., salt—tends to rise up vertically within the gap opening between separating blocks. The simultaneous displacement of blocks in the same downslope direction carries the complete roller in the sense of layer-parallel flow. This brings about the development of a flow cell, within the roller, which corresponds to the vorticity induced by layer-parallel shear. Below the blocks bounding the roller, layer-parallel shear is entirely transformed into internal strain within the salt layer.

Figs. 5b and c show models with synkinematic sedimentation where ductile rollers are buried at two different levels below the sedimentary cover. In Fig. 5b, the roller crests nearly extend up to the surface. In this experiment, a sequential deposition of sand layers is used to simulate sedimentary progradation towards the front of the model to the left. The ductile layer starts to flow before the upper layer is deposited. This explains why up to seven markers are present within the rollers. Passive markers are so intensely sheared before deposition of the upper layer that, when rollers start to develop, they are superposed onto each other in near parallelism with the basement. This provides more detail on the internal structure of rollers. From right to left, the three rollers display an increasing internal asymmetry, whereas their external shape remains nearly symmetrical. The right-hand roller developed under a nearly symmetrical graben, as indicated by the geometry of layers and faults in the sedimentary cover. In addition, the internal structure of the roller is nearly symmetrical,

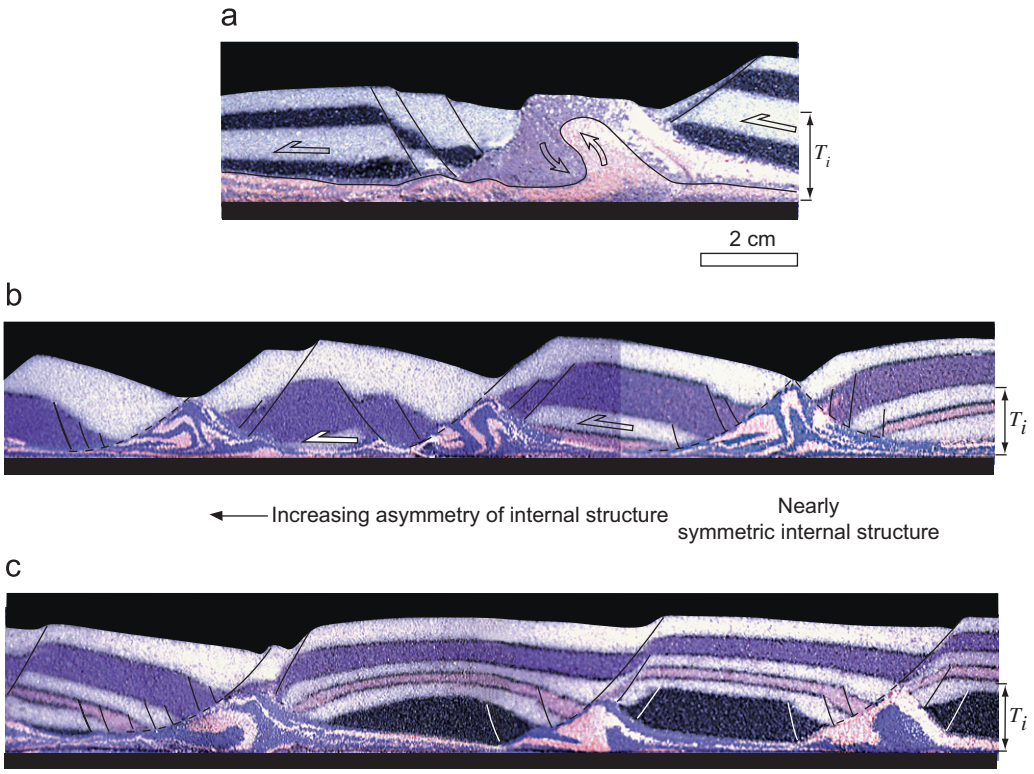

Fig. 5. Internal structure of rollers: (a) roller without synkinematic sedimentary cover, i.e., piercing diapir; (b) nearly emergent rollers and (c) buried rollers. Slab front is to the left. T_i is for the initial thickness of the viscous layer.

with a mushroom-type geometry. The term "mushroom" is here used in a purely geometrical sense and therefore does not imply any uprise of the ductile material into the sedimentary cover as this could occur in classical salt diapirs. In this example, which is exceptional in the present experiments, roller growth occurs in a nearly coaxial deformation environment and, in terms of flow pattern, corresponds to two flow cells with opposite senses of rotation. The two other rollers of the same model show an internal asymmetry increasing toward the left (i.e., towards the front). This is related to the frontward displacement of upper layer blocks with respect to the basement. The internal asymmetry of rollers is accompanied in the sedimentary cover by variations of tilt and thickness in the synkinematic layers and in forward-dipping major faults. The two left-hand rollers are developed below asymmetric grabens. They both display an asymmetric mushroom-type internal structure, indicating a dominant flow cell with a sense of rotation compatible with the dominant sense of shear in the ductile layer and shear along the faults in the cover. In other words, layer-parallel shear tends to enhance flow cells with similar sense of rotation and inhibit the development of flow cells whose sense of rotation is opposite to the vorticity of the layer-parallel sense of shear (compare left side and right side of rollers).

In Fig. 5c, roller hinges throughout the experiment are more deeply buried than in the previous model (Fig. 5b) and the sedimentary pile is thicker. Rollers occur between slightly tilted blocks, but are clearly separated by major normal faults which all dip towards the left. The three rollers exhibit an internal deformation of passive markers, giving rise to asymmetric "internal mushrooms" comparable to those in the previous model and having a similar frontward increase in internal asymmetry.

In the models shown in Fig. 5b and c, it is noteworthy that the degree of internal asymmetry is independent of the external shape and size of the roller. The degree of internal asymmetry clearly increases as a function of upper-layer block displacement with respect to the basement and the resulting amount of finite shear in the décollement layer. The size and shape of rollers is controlled by the relative rate of block separation and synchronous sedimentation.

The close similarities existing between the models without synkinematic sedimentation (i.e., pure diapirism) (Fig. 5a) and with sedimentation (at low rate: Fig. 5b; at higher rate: Fig. 5c) demonstrate that the frontward increase in internal asymmetry in models shown in Fig. 5b and c is a direct consequence of the frontward increase of upper-layer block displacement and, subsequently the intensity of layer-parallel shear in the lower ductile layer.

Fig. 6 shows three examples of growth faults with associated rollovers. At an early stage of development (Fig. 6a), the roller displays an asymmetric mushroom-like internal structure fairly similar to those observed in previous models (Fig. 5). At more advanced stages (Fig. 6b and c), the internal asymmetry is strongly amplified but exhibits deformed patterns of markers

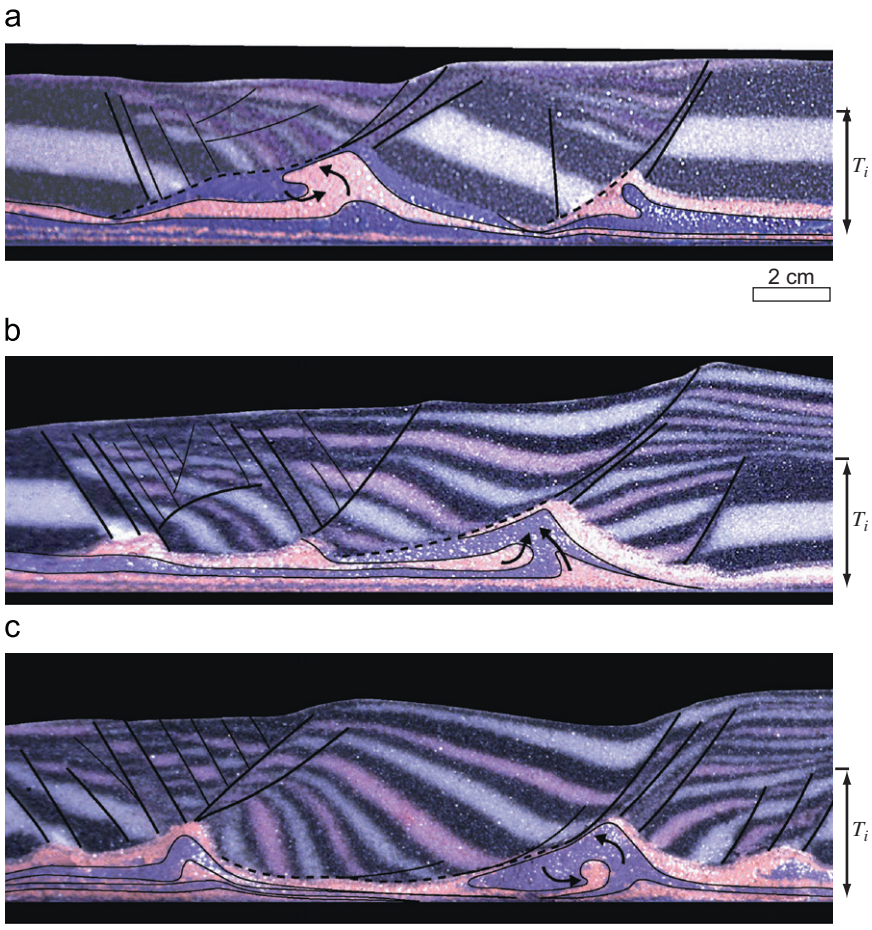

Fig. 6. Rollers associated with growth faults and rollovers: (a) early stage, (b) and (c) advanced stages. Slab front is to the left. T_i is for the initial thickness of the viscous layer.

broadly similar to those in Fig. 6a. During rollover growth, the rollover base comes into progressive parallelism with the basement, thus inducing a strong layer-parallel shear in the décollement layer (Fig. 6b and c). Within the roller, shearing is intense at the base and along the listric fault, while a flow cell remains active at all stages of development.

5. External shape of rollers

In Fig. 7, the aspect ratio W/A of rollers is plotted as a function of the asymmetry ratio W/W_h, where W is the width, A is the amplitude, and W_h is the horizontal projection of the hangingwall limb (h). Two distinct clusters of points represent the rollers associated with tilted blocks and those associated with listric faults and rollovers. The location and shape of each of these clusters reflect the mode of roller development. The arrows indicate the trend of development during progressive deformation.

The ratios W/A and W/W_h decrease during block tilting (see white arrow on cluster). But, because both ratios are dependent on the initial value of W (fault spacing), which is widely variable, the resulting cluster of points is scattered. During growth, the rollover length increases, while the width W of the roller decreases and the amplitude A remains nearly constant. This leads firstly to a decrease in roller asymmetry W/W_h, and secondly to an increase in the

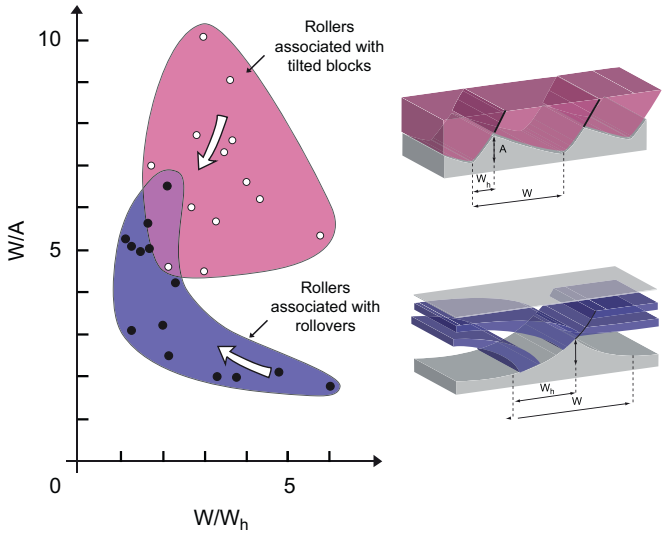

Fig. 7. External shape of rollers. The aspect ratio W/A is plotted against the ratio of asymmetry W/W_h, (with W: total width, A amplitude, W_h: horizontal projection of the hangingwall limb).

aspect ratio W/A. The resulting cluster of points exhibits a boomerang-type shape. It is noteworthy that the development of both types of roller shape is convergent, especially if we consider that they have significantly different lifetimes: short for tilted blocks and long for rollovers.

6. Discussion–conclusions

Our analysis of salt rollers through laboratory experiments leads to the following conclusions:

(1) *Salt rollers result from normal faulting of the sediment–salt interface*. These structures that result from the connection of a fault to the underlying salt layer (Brun and Mauduit, 2008) fall into two sub-categories. When faults are nearly planar with small offsets, rollers develop a triangular shape in section whose aspect ratio and asymmetry are directly dependent on fault spacing, offset and block tilting. With growth faults/rollovers, rollers also take on a triangular shape in section but have upward concave limbs. In the second sub-category, the roller shape tends to acquire a steady-state shape as the fault offset increases.

(2) *The internal structures of salt rollers result from the diapiric-type upward flow of ductile material below zones of normal faulting and thinning of the sedimentary cover, superposed onto bulk horizontal flow within the flat lying ductile décollement layer*. Bulk flow in the décollement layer combines layer-perpendicular shortening with layer-parallel shear, which increases towards the front of the gliding slab. Within rollers, the flow pattern also involves a flow cell whose amount of rotation increases forward from one roller to the next, as a function of layer-parallel shear in the décollement layer. There is therefore a strong dependence between the local internal structure of rollers and the bulk flow pattern in the décollement layer on a larger scale. Incidentally, it is interesting to note that the term "roller" as introduced by Bally et al. (1981) can be considered premonitory even though this concept lacked any explicit kinematic interpretation at that time. The existence of an internal flow cell, revealed in the present experiments, a posteriori fully justifies the term from the point of view of its kinematic implication, as the ductile layer literally rolls within the developing structures.

It is also important to note that the upward flow observed within rollers is not a primary and independent phenomenon due to an inverse density gradient—i.e., Rayleigh Taylor instability—but is merely a consequence of overburden faulting. This is in agreement with similar conclusions previously drawn by Vendeville and Jackson (1992a, b) and by Nalpas and Brun (1993). The upward flow of ductile material below zones of overburden thinned by faulting corresponds to local isostatic readjustment. Strictly speaking, the term "diapir" means ductile intrusion. Vendeville and Jackson (1992a, b) who used this definition (see review by Jackson, 1996), showed that diapirs can rise and fall in thin-skinned extension. Our experiments show that rollers belong to a particular category of diapirs since they do not continuously amplify through time. Their aspect ratios show no significant variation with time or as a function of sedimentation. This suggests that a diapir spectrum exists between those that can attain steady shapes, as a result of layer-parallel shear, and those that change shape due to other bulk strains (Fig. 7).

(3) Rollers represent local zones of salt concentration that produce the usual artefacts on seismic images observed in and around salt structures. A better knowledge of the internal and external structure of rollers could help in defining new procedures of seismic processing to improve seismic images of salt rollers and facilitate seismic interpretation.

Moreover, we believe that the processes of roller development described here are not specific to salt tectonics and can be applied to other types of brittle–ductile systems undergoing extension even at large scale. Comparable structures and flow cells can be expected to occur in the ductile lower crust during late to post orogenic extension. The internal structure of core complex could in some ways be compared to salt rollers.

Acknowledgements

This work was financed by Elf Aquitaine Production, now Total. Experimental data were acquired during the MARGES project (*Modélisation Analogique des Relations entre la Gravité Et la Sédimentation*, Géosciences Rennes-Elf Aquitaine Exploration Production) which aimed to study the interaction between sedimentation and faulting during gravity-driven deformation. The authors acknowledge Schlumberger Geco-Prakla for permission to use seismic data and to publish this paper. We also thank J.J. Kermarrec for invaluable technical assistance during the experiments. Thanks are due to C.J. Talbot, J.T. VanBerkel and S.H. Treagus whose comments helped improving a previous version of the manuscript. Many thanks to the referees I. Davison and C. Faccenna for their extremely useful comments.

Appendix. Patterns of flow and strain in the salt layer

In some recent contributions in salt tectonics, authors have deemed appropriate to refer to two classical fluid dynamics models, the so-called Poiseuille flow and Couette flow, to characterise two end-members kinematic patterns of salt layer deformation (Fig. 8). In the Poiseuille model, the fluid flows through a pipe or between two fixed plates with velocities increasing from the boundaries toward the channel centre. In the Couette model, the fluid accommodates a relative displacement of the channel boundaries: velocities vary linearly between them.

Such flow patterns can effectively be observed within a salt layer as shown by laboratory experiments on brittle–ductile models when the brittle layer lying on top of the ductile layer does not deform. As an example, the flow pattern within the silicone layer in Fig. 2a is very close to a Couette flow. But in most cases, the sedimentary layer lying on top of the salt layer is itself deforming, as illustrated in Fig. 2b where the upper brittle layer is extending. The underlying ductile layer therefore undergoes a combination of layer-parallel shear and layer-parallel stretching. In other words, the salt layer is simultaneously sheared and thinned and consequently the resulting ductile strain combines pure shear and simple shear.

Combinations of layer-parallel shear and layer-perpendicular shortening can lead to a broad spectrum of strain patterns in the salt layer. Fig. 9 presents some of the most common patterns observed in laboratory experiments addressing salt tectonics. Homogeneous strains result from either pure shear or simple shear (equivalent to Couette flow; see Fig. 8) or from their combination. Heterogeneous strain patterns can combine heterogeneous simple shear, whose intensity increases either downwards or upwards, and homogeneous or heterogeneous pure shear. It must be recalled here that, in general, the sedimentary cover extends above the salt layer and that, consequently, the upper boundary of the salt layer is submitted to layer-parallel stretching. Models presented in Figs. 2b and 3 are examples of such combinations of layer-parallel shear and layer-parallel stretching with the amount of stretching increasing in the direction of flow. Layer-parallel shortening can lead to horizontal extrusion dividing the salt layer into two sub-layers with opposite senses of shear.

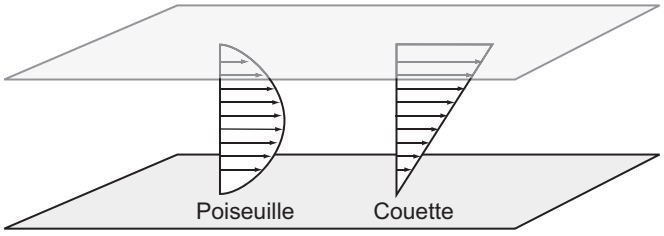

Fig. 8. Poiseuille flow versus Couette flow.

In Fig. 10a, the deformed grid inside the ductile layer of the model shown in Fig. 3 is a typical example of the complex strain variations that can happen in a salt layer below a cover affected by normal faults. A plot of θ_1 (angle between the long axis of strain ellipses and the model basement) against λ_1/λ_2 (ratio of principal axes of strain ellipses with $\lambda_1 > 1 > \lambda_2$) (Fig. 10b)) shows that finite strain results from a combination of layer-perpendicular

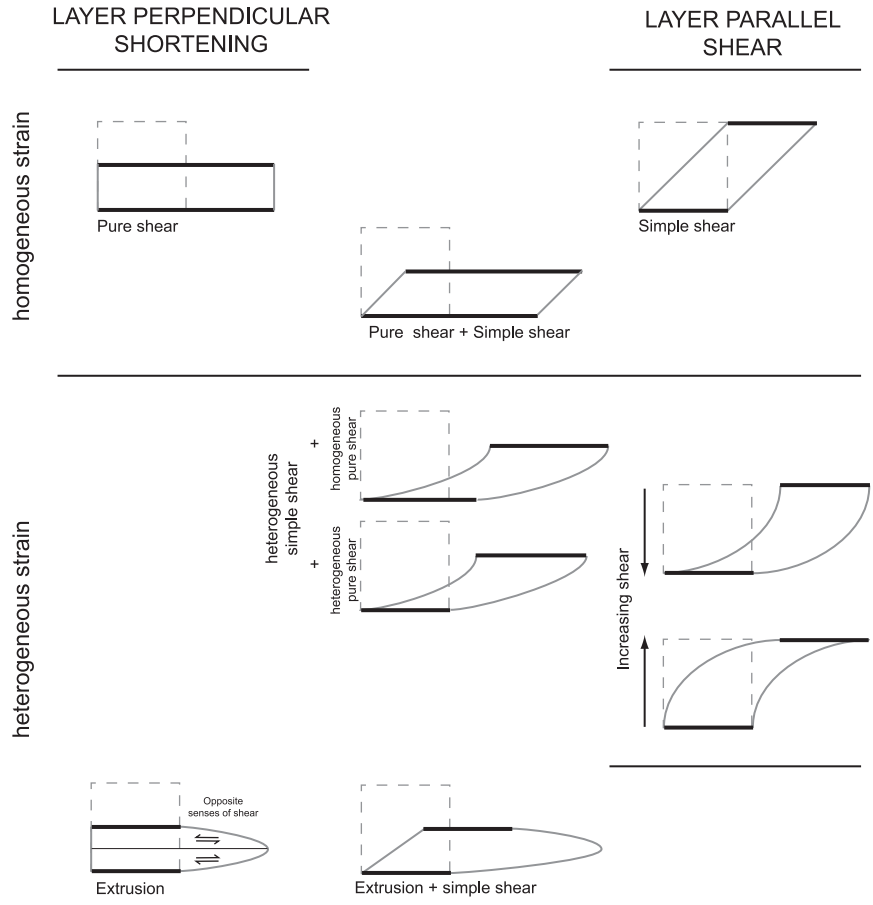

Fig. 9. Some of the most common strain patterns observed in laboratory experiments of salt tectonics resulting from combinations of layer-parallel shear and layer-perpendicular shortening.

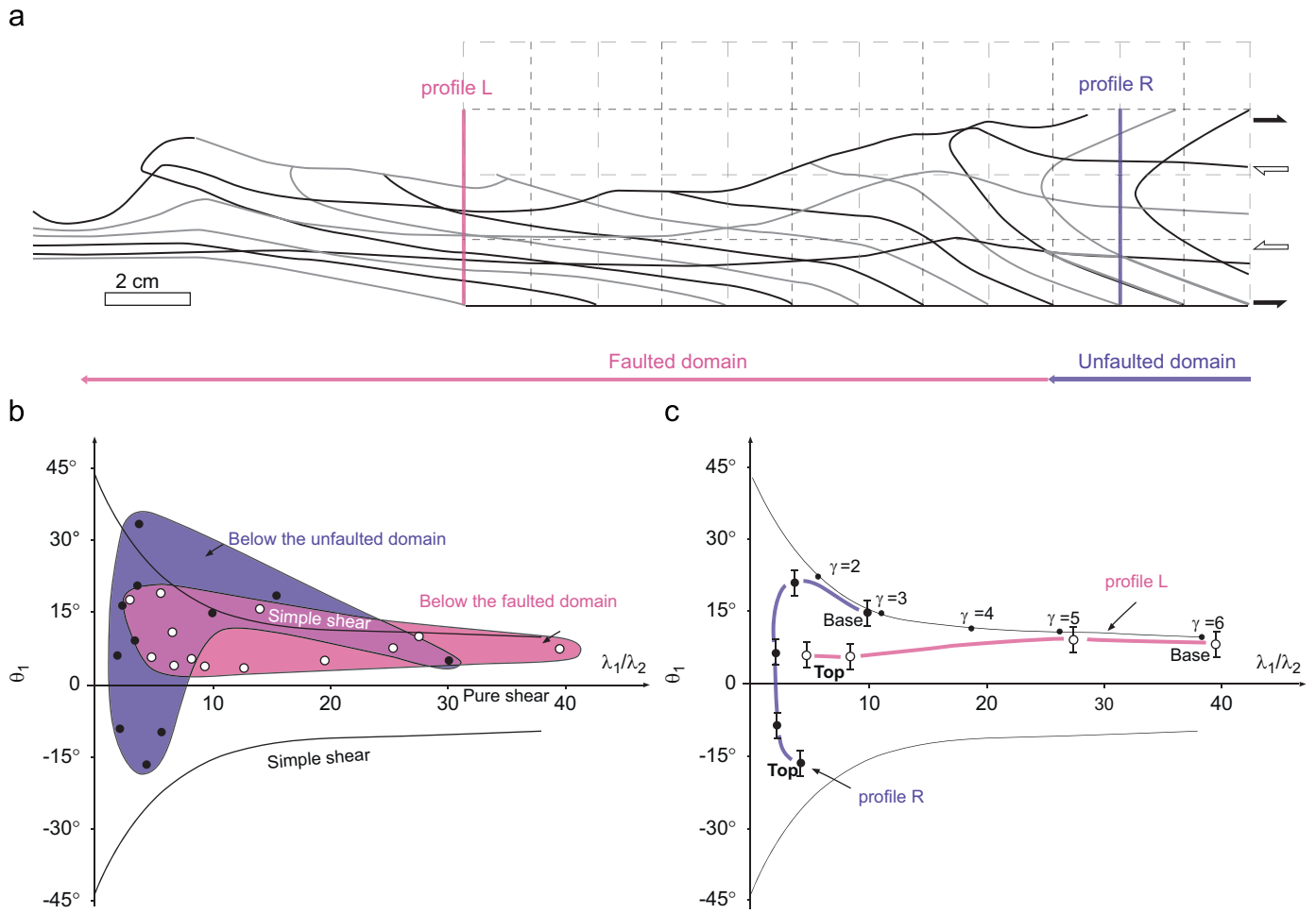

Fig. 10. (a) Analysis of strain variations in the laboratory model presented in Fig. 3a, undeformed (dashed lines) and deformed grid (plain lines) with location of strain profiles under the unfaulted (R) and faulted domain (L). (b) Strain plots of data shown in Fig. 3c where θ_1 is the angle between the long axis λ_1 of the strain ellipse and the model basement and λ_1/λ_2 the ratio of principal axes of the strain ellipse with $\lambda_1 > \lambda_2$. Open and plain circles correspond to strain ellipses located below the faulted and unfaulted domains, respectively. (c) Variations of strain along profiles R and L.

shortening (pure shear) and layer-parallel shear (simple shear) (see Fig. 9). Two vertical strain profiles (Fig. 10c) illustrate the increase in strain intensity (i.e., increasing value in λ_1/λ_2) from top to base below the unfaulted (profile R) and faulted (profile L) domains. In both profiles, the highest strain intensities correspond to simple shear or nearly simple shear. A comparison between these profiles also reveals an increase in strain intensity from back (R) to front (L).

Numerical models of salt tectonics presented by Ings et al. (2005) or Gemmer et al. (2005) display strain patterns that also combine layer-parallel shear and layer-perpendicular shortening. However, a more detailed comparison may be difficult as the boundary conditions used by these authors are significantly different from those used in our models.

References

Bally, A.W., Bernouilli, D., Davis, G.A., Montadert, L., 1981. Listric normal fault. Oceanologica Acta (SP), 87–101.

Brun, J.-P., Fort, X., 2004. Compressional salt tectonics (Angolan Margin). Tectonophysics 382, 129–150.

Brun, J.-P., Mauduit, T.P.-O., 2008. Rollovers in salt tectonics: the inadequacy of the listric fault model. Tectonophysics 457, 1–11.

Brun, J.-P., Merle, O., 1985. Strain patterns in models of spreading-gliding nappes. Tectonics 4 (7), 705–719.

Cobbold, P.R., Szatmari, P., 1991. Radial gravitational gliding on passive margins. Tectonophysics 188, 249–289.

Cobbold, P., Rossello, E., Vendeville, B., 1989. Some experiments on interacting sedimentation and deformation above salt horizons. Bulletin of the Society of Geology France 3, 453–460.

Faugère, E., Brun, J.P., 1984. Modélisation expérimentale de la distension continentale. C.R. Academy of Sciences Paris 299, 365–370.

Fort, X., Brun, J.-P., Chauvel, F., 2004a. Salt tectonics on the Angolan margin, synsedimentary deformation processes. American Association of Petroleum Geologists Bulletin 88, 1523–1544.

Fort, X., Brun, J.-P., Chauvel, F., 2004b. Contraction induced by block rotation above salt. Marine and Petroleum Geology 21, 1281–1294.

Gaullier, V., Brun, J.P., Guerin, G., Lecanu, H., 1993. Raft tectonics: the effects of residual topography below a salt décollement. Tectonophysics 228, 363–381.

Ge, H., Jackson, M.P.A., Vendeville, B.C., 1997. Kinematics and dynamics of salt tectonics driven by progradation. American Association of Petroleum Geologists Bulletin 81, 398–423.

Gemmer, L., Beaumont, C., Ings, S.J., 2005. Dynamic modelling of passive margin salt tectonics. Effects of water loading, sediment properties and sedimentation patterns. Basin Research 17, 383–402.

Ings, S.J., Beaumont, C., Shimeld, J., Gemmer, L., 2005. Salt tectonics at passive continental margins: results from margin-scale. Numerical Models and a Case Study Application from the Northeast Nova Scotia Margin. Abstract for the GAC-MAC-CSPG-CSSS conference, Halifax.

Mauduit, T., 1998. Déformation gravitaire synsédimentaire sur une marge passive. Modélisation analogique et application au Golf de Guinée. Mémoires de Géosciences Rennes, 83, Géosciences Rennes, France.

Mauduit, T., Brun, J-P., 1998. Development of growth fault/rollover systems. Journal of Geophysical Research 103, 18,119–18,136.

Mauduit, T., Gaullier, V., Guérin, G., Brun, J.-P., 1997a. On the asymmetry of turtle back growth anticlines. Marine and Petroleum Geology 14, 763–771.

Mauduit, T., Guérin, G., Brun, J.-P., Lecanu, H., 1997b. Raft tectonics, the effects of basal slope value and sedimentation rate on progressive deformation. Journal of Structural Geology 19, 1219–1230.

McClay, K.R., Dooley, T., Lewis, G., 1998. Analog modeling of progradational delta systems. Geology 26, 771–774.

Merle, O., 1986. Patterns of stretch trajectories and strain rates within spreading gliding nappes. Tectonophysics 124, 211–222.

Merle, O., 1989. Strain models within spreading nappes. Tectonophysics 165 (1–4), 57–71.

Nalpas, T., Brun, J.-P., 1993. Salt flow and diapirism related to extension at crustal scale. Tectonophysics 228, 349–362.

Vendeville, B., 1987. Champs de failles et tectonique en extension: modelisation expérimentale. Thèse d'université, Université de Rennes I.

Vendeville, B., Cobbold, P.R., 1987. Glissements gravitaires synsédimentaires et failles normales listriques: modèles expérimentaux. C. Academy of Sciences Paris 305, 1313–1319.

Vendeville, B., Jackson, M.P.A., 1992a. The rise of diapirs during thin skinned extension. Marine and Petroleum Geology 9, 331–353.

Vendeville, B., Jackson, M.P.A., 1992b. The fall of diapirs during thin skinned extension. Marine and Petroleum Geology 9, 354–371.

Vendeville, B., Cobbold, P.R., Davy, P., Brun, J.P., Choukroune, P., 1987. Physical models of extensional tectonics at various scales. In: Coward, M., Dewey, J.F., Hancock, P.L. (Eds.), Continental Extensional Tectonics. London, 28, pp. 95–107.

Weijermars, R., 1986. Polydimethylsilohexane flow defined for experiments in fluid dynamics. Applied Physics Letters 48, 109–111.